RESEARCH PAPER

Automated monitoring and positioning of single microparticle via ultrasound-driven microbubble streaming

Amirabas Bakhtiari[1] · Christian J. Kähler[1]

Abstract

We present a novel technique that uses ultrasound-driven microbubble streaming for automated positioning of single microparticles of arbitrary size and physical properties in microchannels. We have developed algorithms for automatic detection, tracking, and precise positioning of target particles with arbitrary initial positions across the entire width of microchannels in a live mode that does not require additional structures to precondition the flow for particle positioning. This approach is universally applicable in all areas of microfluidics, regardless of particle size, shape, density, and compressibility. In this study, experiments were performed to position particles of different sizes (2, 5, 10, 15 µm) in 5 lateral regions in a 500 µm microchannel, resulting in valid positioning accuracy for single particles (up to $\mathrm{MAD_f} = 2.3$ µm in a 500 µm).

Keywords Microfluidics · Microbubble · Single particle analysis · Particle positioning

1 Introduction

The manipulation of microparticles and cells plays an important role in numerous medical and biological applications. Over the last decade, advances in microfluidics have enabled wide range of functions such as the recognition, focusing, mixing, counting, lysis, and analysis to be performed on individual cells utilising lab-on-a-chip devices (Nilsson et al. 2009; Nan et al. 2014; Sheng et al. 2014; Mernier et al. 2010; Yang et al. 2006; Zhao et al. 2013). The enrichment of circulating tumor cells (CTCs), hematopoietic stem cells (HSCs), and circulating fetal cells (CFCs) (Armstrong et al. 2011; Wognum et al. 2003; Bischoff et al. 2003; Chen et al. 2014), along with single-cell impedance spectroscopy (Han and Frazier 2006; Cho and Thielecke 2007; Chen et al. 2011; Malleo et al. 2010), and single-cell electroporation (Khine et al. 2005) are only a few examples of cell isolation, which underlines the importance of biological cell and single particle manipulation.

Active cell manipulating applications typically use external fields such as acoustic, electric, magnetic, or optical fields to apply forces to displace cells (Shields et al. 2015). In acoustofluidics, particle manipulation in a microchannel is typically performed by using bulk acoustic standing waves (Augustsson et al. 2016), surface acoustic waves (Collins et al. 2015), and acoustically actuated microbubbles whereby the bubble oscillation can generate counter-rotating vortices (Riley 2001; Marmottant and Hilgenfeldt 2003; Versluis et al. 2010). Acoustically actuated microbubbles in microchannels are a biocompatible method for cell manipulating where the change in frequency and amplitude of actuation can easily control the streaming flow, resulting in precise control of the particle manipulation (Ahmed et al. 2016; Rallabandi et al. 2014; Wang et al. 2013), whereas this would be a challenging task in applications using an on-off method of the uncontrolled force fields that can only deflect particles from mainstream to the waste (e.g. using highly focused high-frequency traveling SAW (Collins et al. 2016) or cavitation a bubble in PLACS (Chen et al. 2014)). In our previous studies, extensive investigations of microbubble streaming showed that it can be effectively used to mix microparticles. As a next step, we wanted to tackle another important goal of our project, namely to find out whether this non-invasive streaming can also be used to position particles instead of mixing them. Although

✉ Amirabas Bakhtiari
amirabas.bakhtiari@unibw.de

[1]   Institute for Fluid Mechanics and Aerodynamics, Fakultät für Luft- und Raumfahrttechnik, Universität der Bundeswehr, Werner-Heisenberg-Weg 39, Neubiberg 85579, Bayern, Germany

in some studies particle manipulation via microbubble streaming has been discussed in some studies (Patel et al. 2012; Thameem et al. 2016) and streaming of microbubbles by continuously actuating the piezo element has been used for particle separation of size-dependent particles, here we activate or deactivate the piezo element based on the current particle position independently of particle size or compressibility. So that an operator can effectively specify the single particle positions at the preferred time in the live mode, which would be essential when isolating rare cells or removing unwanted contaminants in a flow. In this way, positioning does not depend on specific particle properties such as size, shape, density, compressibility, etc., making this approach universally applicable in all areas of microfluidics. Since the concept is not based on moving parts but only on an oscillating bubble, the positioning device is robust and does not require any special maintenance or cleaning, and can be easily integrated into various applications. However, the precise and rapid operations on lab-on-a-chip devices, which integrate various functions on a miniature chip, highlight the essential need for an advanced control system and a reliable, fast control system that can improve the accuracy and speed of cell manipulating in microfluidic applications.

In this study, we present a novel autonomous technique for precisely positioning single particles across the width of the microchannel by ultrasound-driven microbubble streaming. To achieve this, we integrate open-loop control algorithms into the operation and demonstrate precise active cell positioning. Using our control system, particle positioning is performed for each microparticle individually with an arbitrary starting position, without the need for preliminary focusing or flow conditioning before positioning. This technique incorporates the control algorithms and various functionalities to detect the initial position of a target single particle, apply the microstreaming at the right time by triggering the piezoelectric input, and track the target to reach its final position with an accuracy of up to tens of micrometers, whether the final position is manually set by the operator or automatically defined by the movement of the mouse pointer in live mode.

This technique can be used to remove unwanted contaminants from flow or to isolate single biological cells or other contaminants based on their physical properties, which requires a single-cell suspension. Therefore, biological cell samples must be processed into a single-cell suspension prior to flow cytometric analysis. There are a number of protocols that involve mechanical dissociation or enzymatic digestion of the sample, but these are beyond the scope of this work. However, the analysis of bacteria is not only important for blood analysis but also crucial for other microbiological studies, such as wastewater treatment and analysis, the formation of bio-barriers to prevent

groundwater contamination, etc (Vrouwenvelder et al. 2009; Klapper and Dockery 2010; Flemming 1997; Creber et al. 2010; Tchbanoglous et al. 2003).

2 Experimental setup

This section describes the experimental setup, which generally consists of three main parts: a microfluidic system, an optical setup, and the control system. To reduce measurement errors, the entire setup is mounted on an anti-vibration table.

2.1 Microfluidic chip

A schematic of the microchannel and flow control system is displayed in Fig. 1. In this work, experiments are performed in a PDMS microchannel containing a side pit to trap a cylindrical microbubble by Poiseuille flow (Toghraie Semiromi and Azimian 2010; Rahmati et al. 2018). The microchannel of height $H = 100\,\mu m$, width $W = 500\,\mu m$, and length $L = 20$ mm has a side pit of width $w = 80\,\mu m$ and length $h = 200\,\mu m$ (Fig. 2). Following the previous studies (Wang et al. 2013; Rallabandi et al. 2014; Ahmed et al. 2016; Tovar and Lee 2009; Ahmed et al. 2009), the width of the cavity was chosen so that it is not too wide in order to avoid significant 3D flow phenomena around the bubble, and not so narrow that it creates a very small bubble with a minimal effect on the flow field. The microfluidic chip was fabricated by the standard soft-lithography method, analogously to the approach described by Wang et al. (2012). For the experimental study, the microchannel was filled with an aqueous glycerol solution containing fluorescent polystyrene
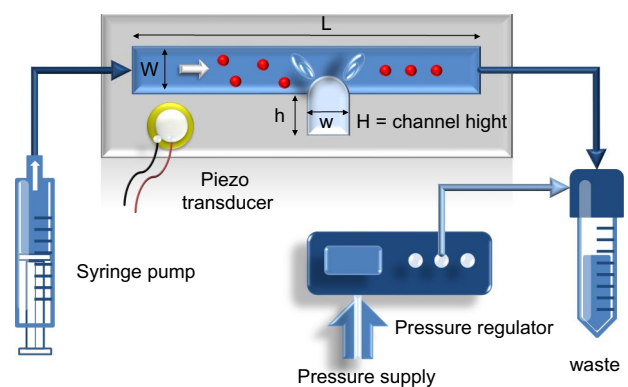

Fig. 1 Schematic of the microchannel and flow control system. PDMS microchannel of width W, height H, and length L has a side pit of width w and length h. The microbubble is excited by a piezo transducer and generates a primary oscillating flow that leads to a secondary flow in the form of counter-rotating vortices. The flow rate is adjusted by the syringe pump, and the pressure regulator tunes the pressure of the liquid to stabilize the bubble
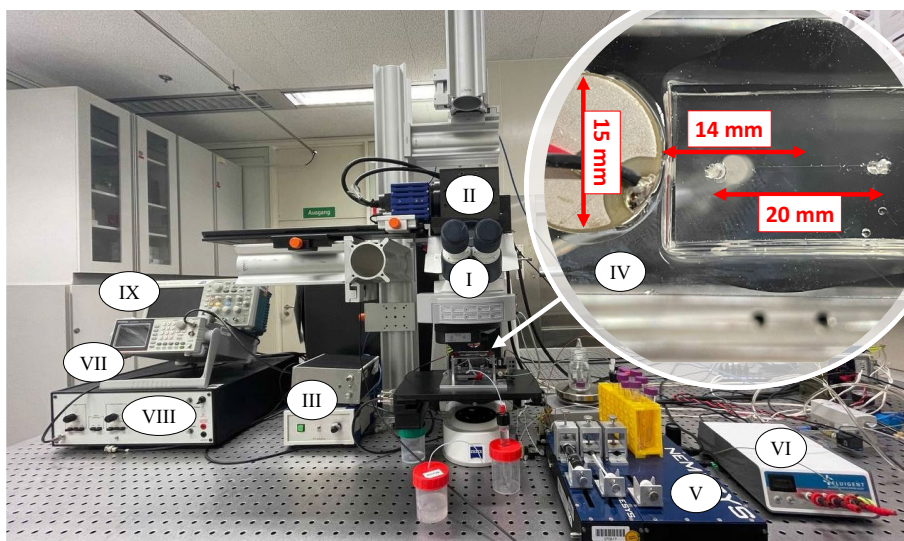
Fig. 2 The devices of the experimental setup are divided into three main parts: a microfluidic system, an optical setup, and the setup for the control system. The optical setup consists of an upright microscope with a 10× objective (I), a camera (II), and light sources (III). The microfluidic setup includes the microfluidic chip, which consists of a piezoelectric element placed at a distance of 14 mm from the cavity in the center of the 20 mm long microchannel (IV), a syringe pump (V) that drives the flow into the channel, and a pressure regulator (VI) to control the bubble size. Finally, the piezo transducer is actuated using a function generator (VII), an amplifier (VIII), and an oscilloscope (IX) controlled by LabVIEW

particles with a diameter of 2.24 µm (Fluored Particles, Microparticles GmbH, Germany). The glycerol content of 23.8 % (w-w) in the aqueous glycerol solution was used in this work to obtain buoyant particles for particle positioning. The sample flow is driven into the channel in a controlled manner by means of a syringe pump (neMESYS) and a pressure controller (FluigentMFCS™-EZ, 0-1000 mbar, France).

2.2 Optical setup

The microfluidic chip is located on the three-axis motorized stage of an upright Zeiss AxioImager.Z2 microscope equipped with a 10× objective (EC Plan Neouar 10× /0.3 M27) to which an sCMOS camera (pco.edge 5.5) is mounted (see Fig. 2). A continuous laser, high-power LED, or halogen light can be used to illuminate the particles in the flow so that an optical recording with the camera can be possible (see Fig. 3).

2.3 Control system setup

Lab-VIEW (National Instrument, USA) is used to simultaneously control image acquisition, image analysis, and particle positioning in live mode with a custom-made feedback system. The feedback control system consists of a function generator (GW INSTEK AFG-2225), an amplifier (Krohn Hite 7500), and an oscilloscope (Teledyne LeCroy HDO6104) to send a predefined electrical signal to the piezoelectric transducer which is mounted to
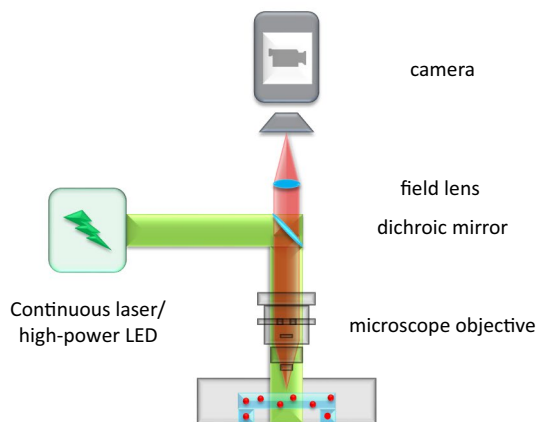

Fig. 3 The optical setup includes an upright Zeiss AxioImager.Z2 microscope equipped with a 10× objective (EC Plan Neouar 10× /0.3 M27) and a CMOS camera (pco.edge 5.5), using continuous laser and high-power LED for fluorescence microscope

the microfluidic chip (see Fig. 2). The function generator is triggered by a National Instruments USB-6002 DAQmx data acquisition device that receives commands from LabVIEW (Fig. 5). When the program is started, the predefined camera settings (FOV size, exposure time, frame rate,...) are sent to the camera, and image acquisition starts (see Fig. 4).

The next step is the segmentation of the images into ROIs. The origin, width and height of the ROIs are calculated based on the channel dimensions, bubble position and the target position, which can be defined manually in

Fig. 4 Flow chart of the particle positioning algorithm (Lab-VIEW). ROIs are defined based on test setup parameters: y_c represents the width of the channel, y_t target position, x_b center of bubble, $2a$ width of the cavity, and e gap between upward and downward flow (in this study $e_1 = e_2 = 100\,\mu m$ based on flow characterization Fig. 6)

Data acquiring

start

Imaging (in FOV) ← Set camera

Display FOV

AS on/off

Particle positioning

Thresholding Manual/ Automatic

Particle detection
- Find circles
- Find particle

Data optimization/ Filtering (FOV to ROI) → Preprocessing/Binarization →

ROI definition

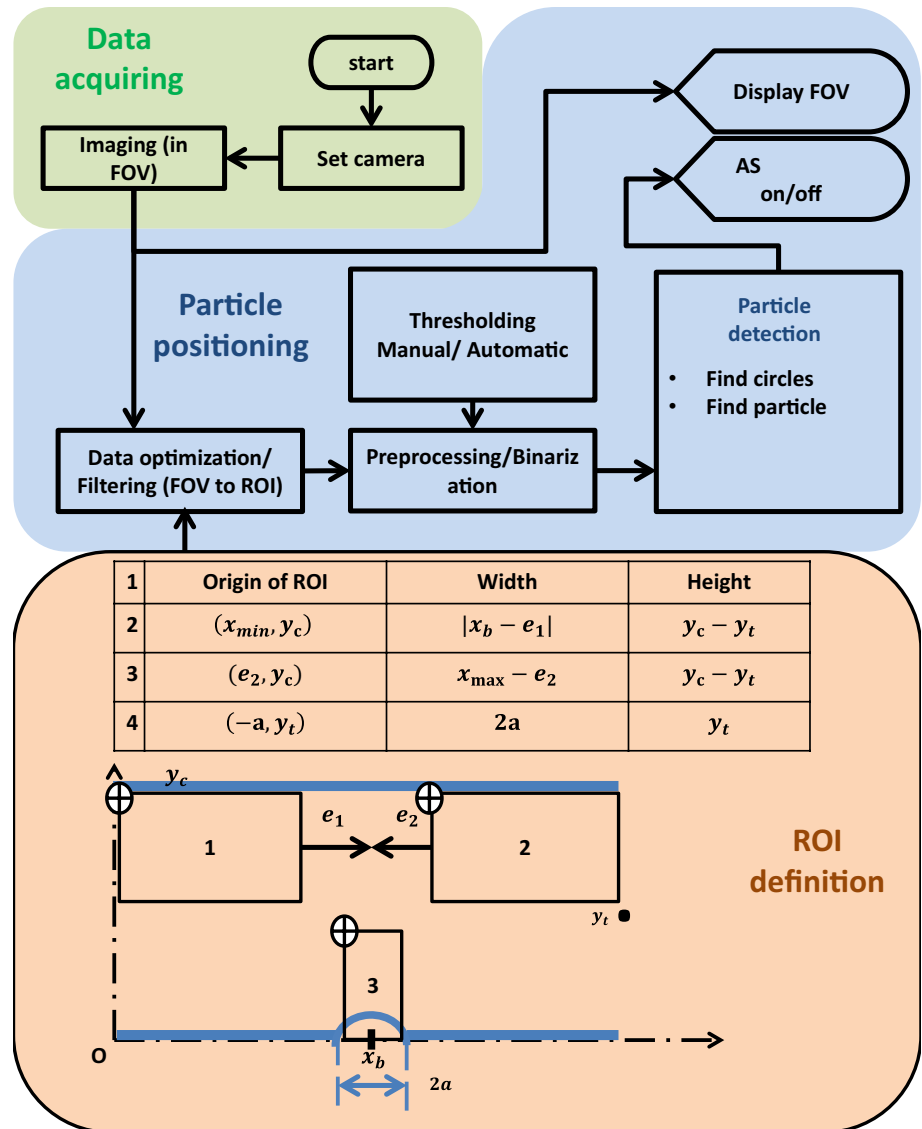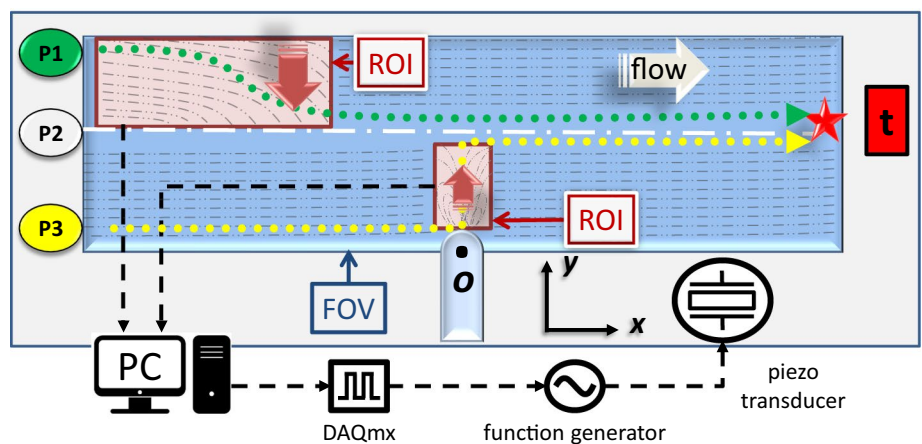|	Origin of ROI	Width	Height
1			
2	(x_{min}, y_c)	$|x_b - e_1|$	$y_c - y_t$
3	(e_2, y_c)	$x_{max} - e_2$	$y_c - y_t$
4	$(-a, y_t)$	$2a$	y_t

Fig. 5 Schematic of the control system for positioning individual particles with different positions ($y_{p\text{-green}} > y_t, y_{p\text{-white}} = y_t, y_{p\text{-yellow}} < y_t$). The microbubble is activated by the piezo transducer when a particle is detected in the ROIs (red rectangles), which are extended to the entire width of the channel, except at the target level. The generated streaming evicts the particles from the ROIs to reach the same level as y_t

P1 P2 P3 ROI flow t

FOV

PC

DAQmx   function generator   piezo transducer

LabVIEW or automatically by reading the target position (y_t) of a mouse pointer as it moves (up and down) on the FOV display. After this step, the reduced data is converted into binary data by applying an appropriate threshold and inversion, in the case of bright field imaging. The proper threshold can also be set manually or automatically in the presence of a sample particle in the FOV. Then, the particles are detected, analyzed and tracked by different sub-algorithms (such as a particle finder or circle finder,...) and important parameters such as dimensions and positions... are extracted to be used for further processing. e.g. sending digital signals (triggering) to the function generator to send the predefined signal (resonance frequency of the microbubble) to the piezoelectric. For monitoring purposes, the original images of the FOV and binary images of the ROIs are displayed on the control panel. These images can be stored temporarily in the camera's RAM or permanently on a hard disk for further data analysis.

3 Methods

The investigation of single particle positioning using a feedback control system represents the most important part of this work. In this section, the bubble stabilization in a steady-state flow, particle detection, and positioning methods are discussed.

3.1 Stabilized bubble in steady-state flow

The presentation of a steady-state flow together with a stabilized microbubble is intended to examine the proposed technique in detail. Rapid filling of the microchannel with liquid causes an air pocket to be trapped in the side pit that creates a quasi-hemicylindrical microbubble. PDMS as a porous medium is highly permeable to gases (Xia and Whitesides 1998). Depending on the relative pressure difference between the bubble and the external environment, the inflow or outflow can cause the bubble to grow or shrink (Volk and Kähler 2018). Volk *et al.*(Volk et al. 2015) could overcome this issue in a stationary fluid by developing a proportional–integral–derivative (PID) controller that controls the equilibrium of gas transport. To adapt their approach to stabilize the micro-bubble for combined Poiseuille flow with bubble streaming, the syringe driver was added to the system to control the flow rate, while the hydrostatic pressure was kept constant by the pressure controller. In this fashion, any desired Poiseuille flow rate is achieved with a syringe pump, and at the same time, the pressure regulator can tune the pressure in the channel (Fig. 1).

3.2 Particle detection

Particle detection and recognition processing is the first task in particle positioning. This provides feedback to the control system and consequently to the actuator for positioning the particles throughout the entire operating time. To achieve high resolution and interactive particle positioning, the frame rate of the sCMOS camera in the live mode is set to 100 Hz for the flow velocity studied here. To obtain a smooth data computation in live mode, image processing is applied only to small regions of interest (ROI) inside the FOV, as indicated in Fig. 5. Depending on the size, shape, and content of the particles and the basis of the method (machine learning-based, predefined control algorithms, etc), different approaches can be used to identify the target particles. In this study, the control algorithms are developed independently of each other so that any other particle detection method can be easily integrated into the control system.

Depending on the application, different types of light sources can be used with different particles. It is our understanding that there is a great interest in the detection and processing of biological cells larger than 2 µm (2.24 µm), such as yeast cells (typically 3–4 µm), due to their morphological characteristics. The particle size of 2 µm/s was chosen as the lower interval of a range to ensure successful particle detection for larger particles. In our laboratory for epifluorescence microscopy, we have different illumination light sources available, such as high-power LED, green laser, and filtered light of a mercury lamp (green light). However, due to the high light fluctuation rate of a mercury lamp (300 Hz), the use of laser or LED light is preferred. The illumination of fluorescent particles provides a high SNR where the emitted particle appears in the dark background field of view. In this case, most unwanted features, be it impurities in the fluid or channel contamination, are automatically filtered out in the very first steps and do not find their way into the processing algorithms, which significantly reduces the processing time and errors.

However, this technique is not always applicable, for example when the cells of interest are not fluorescent or a higher imaging rate with a significantly shorter exposure time is required, using higher light intensity might be too strong for the microscope optics or the cells. To overcome this limitation, shadowgraphy using background illumination can be used as an alternative method when epifluorescence is not practical (e.g. Volk et al. (2019)). The recorded images are later inverted to use the same image processing as with epifluorescence. In this way, using a 100 W halogen lamp can significantly increase the brightness of the recorded images. This allows us to reduce the exposure time from 1 ms to 3.8 µs, so that the camera can record at higher frame rates. The same bright

field processing also performed for particles of different sizes (2, 5, 10, and 15 μm), resulting in a valid signal-to-noise ratio (at least 5 for 2 μm particles).

Whether in darkfield or brightfield mode, the particles are either brighter or darker than the background and there should be no problem as long as the objects in the flow do not perfectly match the index of refraction of the flow medium. Therefore the target particles can be always identified reliably by thresholding, background removal, and binarizing the ROIs of the recorded images.

4 Results and discussion

4.1 Effective streaming range

In the technique we propose, the secondary microstreaming flow caused by resonant ultrasonic actuation of microbubbles is considered to be the operator that mobilizes the target particles to the desired lateral position across the width of the microchannel. To achieve fast particle displacement by the shortest path, the strangest vortices with minimal complexity are preferred. Volk and Kähler (2018) showed that the fastest streaming occurs in the first resonance mode when the protrusion depth of the bubble equals a quarter of the width of the cavity ($d = 0.5\, a$, a is half of the width of the cavity).

To determine the effective range in which the flow can significantly mobilize the particles, the combined Poiseuille flow with the bubble streaming was characterized for the first resonance mode under steady-state conditions for different voltage amplitudes of the piezo transducer. The experimental conditions were considered similar to those used for particle positioning. General Defocusing Particle Tracking (GDPT) Barnkob et al. (2015) was used to track the 2 μm tracer particles in the combined Poiseuille flow (from left to right) with the streaming flow when the microbubble ($d = 0.5\, a$) oscillated by applying $v_r = 75$ V_{pp} at its first resonance mode $f_r = 18.9$ kHz (Fig. 6). Results show that the flow field is separated into two main regions by a separatrix (shown in red). Particles above the separatrix can not reach the streaming loops near the bubble and return downstream of the microchannel to almost the same initial lateral level as upstream (see Fig. 6). It was observed that as the peak-to-peak voltage on the piezoelectric element increases, the separatrix line moves towards the center of the channel until a critical value is reached, beyond which the bubble detaches from the cavity - resulting in loss of bubble streaming. Therefore, the peak-to-peak value was chosen here just below the critical value (75 V_{pp}).
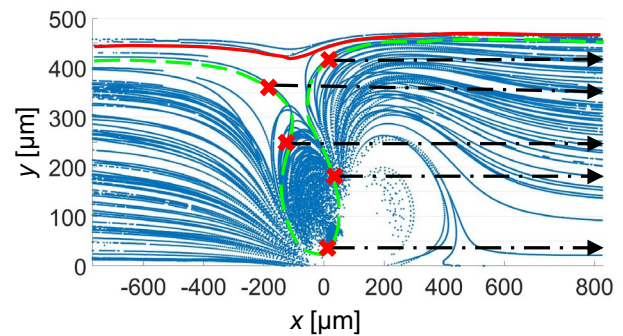

Fig. 6 Tracking of 2 μm particles in a combined Poiseuille flow (left to right) with the streaming flow when the microbubble ($d = 0.5\, a$) oscillated by applying 75 V_{pp} at (18.9 kHz). Particles above the separatrix (red line) cannot reach the loops and then return downstream of the microchannel to nearly the same initial lateral level, unlike particles below the separatrix, which can be trapped in the counter-rotating vortices and reach any lateral position in these loops. The green dashed line is the path of the last trapped particle ($y_{i,\max}$) by the counterrotating vortices in the y-direction where the particles below this line can be mobilized and released at any point (e.g. red crosses) and maintain their y-position for the rest of the way (black dashed arrows)

4.2 Operating principle

As shown in Fig. 5, the center of the microbubble is considered the center of the coordinate system, with the x-axis defining the streamwise direction, and the y-axis defining the spanwise direction. In this schematic y_p stands for the lateral position of an incoming particle and y_t stands for the final position where the particle should be located in the y-direction. The main goal is to laterally transfer the particle from y_p to y_t within the effective streaming range. To address this issue, the transducer remains off (passive mode) and is only turned on (active mode) if an incoming particle with a y_p other than y_t is present in any of the ROIs. If y_p is different from y_t, the microbubble is activated to create the streaming for the movement of the particle up or down until it reaches the same level as y_t. At this moment the microbubble should be turned off so that the particle remains in the y_t level for the rest of its path (see e.g. Fig. 8).

Particles with Stokes number smaller than one (Stk<1) closely follow the streamlines of the fluid and exit the ROI on the horizontal side, which is aligned with the y_t level (see Fig. 5). However, it takes longer for particles with Stk>1 and in some cases with Stk >>1 and faster Poiseuille flow (insufficient operating time), the particle may not fully reach the y_t level and exit the ROI on the vertical side.

The exact dimensions and positions of the ROIs are highly dependent on flow rate, microbubble streaming, particle size, target position, etc. In general, a measurement of streaming flow (Fig. 7) can identify the area with upward or downward flow features that help to accurately arrange the optimal configuration of ROIs for a particular target location. Generally,
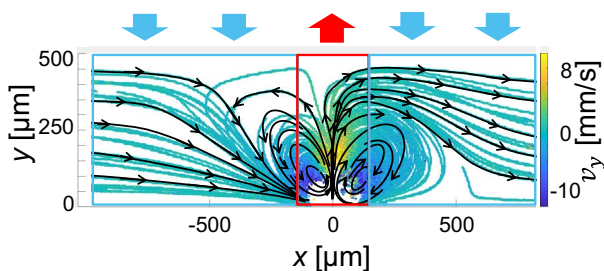
Fig. 7 Measured combined poiseuille flow with streaming flows of cylindrical microbubbles at an actuation frequency $f_r = 18.9$ kHz with $V_r = 75$ V$_{pp}$. Fast upward streaming is located in a narrow region ($-100 < x_{upward} < 100 \, \mu$m) above the microbubble (red rectangle). Relevantly slow downward streaming regions are determined upstream and downstream of the microbubble
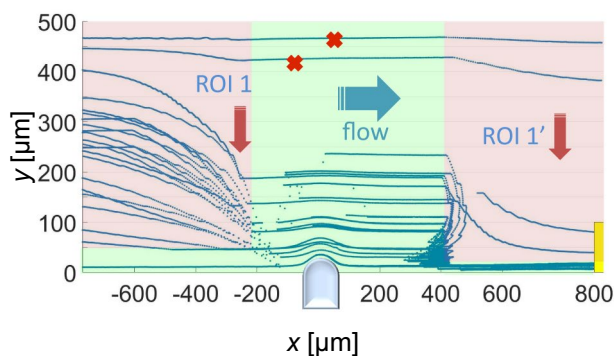

Fig. 8 Case 1, two ROIs (red rectangles) are used to detect and focus the particles near the wall within the range of $0 < y_t < 100 \, \mu$m (yellow band). Red arrows in the ROIs show the y-direction of the flow when the bubble is actuated. In the green area the piezo is off. The blue paths show particle focusing paths. Two particles (red crosses) could not be directed because of the long distance from the bubble

the area upstream and downstream of the bubble with sufficient distance between the loops (depending on the flow velocity, in this work $e_1 = e_2 = 100 \, \mu$m) is suitable to bring the particles down, with the flow directed downward. The downward flow upstream of the bubble is focused on the center of the bubble, which is faster with a higher gradient than the downward flow downstream of the bubble and can also carry the particle to the level up to the surface of the bubble, while the same level cannot be reached by the downward flow downstream of the bubble. Strong upwards streaming right above the actuated bubble is considered to push the particle out of the bubble in the positive y-direction. Due to the fast flow in this area, the positioning takes less time than in the other regions, therefore the width of the ROI can be chosen as relatively small to avoid unwanted trapping of the particles in the counter-rotating vortices. Thus individual ROIs, acting as virtual sensors, span the entire width of the microchannel in the effective streaming region (see Fig. 4),

starting from the top wall to the y_t-level in the downward flow regions ($0 < H_{ROI_{up}} < y_t$) and from the y_t-level to the bottom wall in the upward flow region ($y_t < H_{ROI_{down}} < y_{max}$). The y_t-level itself is defined as a narrow region (10 μm in this study), so particles entering this region are considered correctly positioned and the system is deactivated. The target itself can be defined manually by entering the y-position in the front panel of LabVIEW or getting the coordinates of the mouse pointer when it is moved within the FOV in live mode. In this case, the ROIs are set automatically to bring the particles to the same lateral level as the mouse pointer in live mode.

However, adding an ROI downstream of the bubble to bring down the particle may increase accuracy in a case where the particle could not successfully reach the target level by passing from the first ROI (see Fig. 8). In any case, if a particle cannot reach the target within one or more ROIs, the algorithm deactivates the operation as soon as the particle leaves the ROI.

4.3 Active particle positioning

4.3.1 Experiments

This technique was developed using one microbubble that aims to position a single particle or isolate one rare cell at a time (one particle at a time in the FOV). For this reason, a low concentration of 2 μm particles in the solution (glycerol-water 23.8% w/w) was used in this study, and data with the presence of more than one particle at a time were excluded from the calculation. Experiments were performed to determine the uncertainty of positioning the single particles within 5 distinct regions of 100 μm along the width (y-direction) of the microchannel with a width of 500 μm, and height of 100 μm. This could be a good estimate for practical applications with a 500 μm microchannel, where an operator can freely direct a single particle into one of the 5 outlet channels. Experiments were carried out using a microbubble ($w = 80 \, \mu$m, $d = 0.5$ a) oscillating at its first resonant mode $f_r = 18.9$ kHz and $V_r = 70$ V$_{pp}$. The particle solution is propelled into the channel by the syringe pump (0.014 μl/s) and the bubble surface height is controlled by regulating the outlet pressure between 6 and 8 mbar above atmospheric pressure. On average, each run took about 20 min at 100 frames per second, so an average of 24 valid individual particles were captured in each case.

In case one (C1), the particles are focused near the wall within a range of $0 < y_t < 100 \, \mu$m downstream of the channel by placing one ROI upstream and another downstream (Fig. 8), resulting in a focusing with a median value of $\tilde{y}_{p_f} = 14 \, \mu$m and median absolute deviation of

$MAD_f = 2.3\,\mu m$. In this case, since it is not necessary to push the particles against the opposite side of the bubble, both ROIs are in the region where the only downward flow is present, with ROI1' being taller to converge the particles more near the wall. As can be seen from the tracked particles (blue paths), ROI1' significantly supports focusing the particles that did not fully reach the target level when passing through ROI1. It can also be seen that the two particles with $y_p > 400\,\mu m$ (red crosses) could not be directed because they are far from the bubble, where the streaming is relatively slower than at the lower levels, which are closer to the bubble.

In the next step, in case two (C2), the particles are brought down and up by ROI1 and ROI2, respectively, to position them in a range of $100 < y_t < 200\,\mu m$. The same procedure is performed for case three and case four for the ranges $200 < y_t < 300\,\mu m$ and $300 < y_t < 400\,\mu m$ (resulting $\tilde{y}_{p_f}$ of 150.14, 253 and 364.7 μm with MAD_f of 14.7, 24.6, and 30.5 μm for C2, C3, and C4 respectively). In these three cases, ROI2 is located just above the bubble, i.e., in the region where there is an upward flow that lifts the particle to the target level. In case 5, particles are positioned in the range of $400 < y_t < 500\,\mu m$, near the wall in front of the bubble. Since no downward flow is used in this case, only a single ROI is placed near the center of the bubble where the fastest upward flow is available to bring the particle to the farthest lateral plane of the microchannel, resulting in positioning with a median value of $\tilde{y}_{p_f} = 429.4\,\mu m$ and median absolute deviation of $MAD_f = 29.4\,\mu m$.

The results for all cases are shown in Fig. 9. The use of two ROIs in case 1 ($0 < y_t < 100\,\mu m$) shows that the use of downward streaming upstream and downstream of the microbubble can significantly increase the positioning accuracy. Besides, the large range of downward flow (ROIs in Fig. 8) provides more time to bring the particles down (negative y-direction) which provides the highest accuracy among all the cases. In cases 2, 3, and 4, the combination of downward and upward streaming is used and the results show that particles are properly located in the target ranges. Unlike case 1, where more space, time, and a slower downward flow were available, correspondingly fast upward flow in this narrow region above the microbubble limits the time to accurately lift the particles to the target level. Therefore with small movements back and forth from the center of the bubble ($x_b = 0$), slower upward streaming can be provided for positioning the particle in the lower level of the microchannel. However, the size and location of ROI2 should be tuned within a range of $-100 < X_{ROI2} < 100\,\mu m$ where the upward streaming is present. Since in case 2, most incoming particles should still be brought down rather than up, just as in the first case, downward streaming can provide decent accuracy in this case. In case 3, the chance of bringing the incoming particles up and down to the center of the channel is almost equal. In this range, the upward flow is still fast and the effect of skipping the fast-rising particles from the target area may slightly reduce the positioning accuracy compared to the other cases. To overcome this problem, ROI2 shifts slightly (to the left or right) from the center of the bubble where the upward flow is slower. Although more particles should move up than down in case 4 compared to the previous case, the slower upward streaming for this range (farther than the bubble) causes higher accuracy than in case 3.

4.3.2 Additional ROIs

To further increase the positioning accuracy (in cases 2, 3, and 4), similar to the first case, another ROI (ROI1') was added to the region of downward flow downstream of the bubble. This allows the particles that could not be accurately positioned by the previous ROIs to have another chance to approach the target. The red error bars show the improved results in cases 2, 3 and 4 (Fig. 9). And finally, case 5 ($400 < y_t < 500\,\mu m$) where all particles should be located near the front wall of the bubble. To use the full capacity of upward streaming the ROI is located exactly at the center of the bubble ($X_{ROI} = X_b$), where the fastest streaming exists.
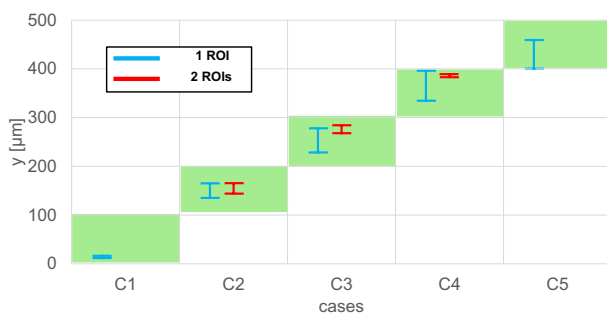

Fig. 9 The median value and median absolute deviation of the 5 cases (blue error bars). Green rectangles show the target range for each case. Red error bars show the improved results when using additional ROI downstream of the bubble
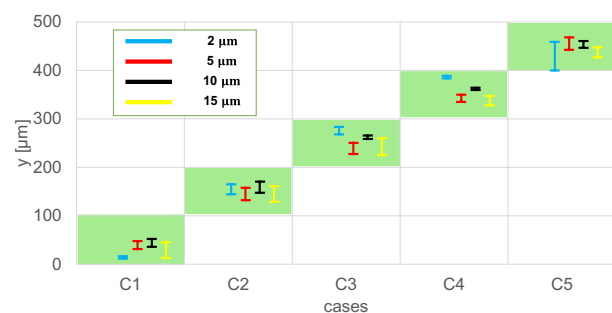

Fig. 10 The median value and the mean absolute deviation of the 5 cases for the particles with different sizes (2, 5, 10, 15 μm)

The results of case 5 also show the limit of particle positioning in this work to determine how accurately and far away from the bubble particles can be localized.

4.3.3 Larger particles

As mentioned earlier, positioning can take longer for larger particles with a higher Stokes number. Figure 10 shows the comparison between the results of 2 µm particles with the results of a series of experiments that were performed with 5, 10, and 15 µm particles at $V_{mean} = 268$ µm/s (the quantitative values can be found in the supplementary). As can be seen, in each case, although the positioning accuracy differs slightly, no dramatic changes in MAD_f for larger particles are observed compared to the results of positioning 2 µm particles, and the particles with a valid accuracy were successfully positioned in the target areas (green area). The differences in median values can be optimized and aligned to the center of the target area by moving the ROIs slightly up or down so that more particles are placed in the desired area. In general, positioning of larger particles is not a problem as long as sufficient operating time (duration of particle present in the ROI) is available, which can be limited by increasing the flow rate.

4.3.4 Different flow rates

Although the system must be tuned at the beginning of each new test condition (new flow rate), the previous experiment was repeated for two higher flow rates, keeping all control parameters (positions and dimensions of the ROIs) constant and increasing only the flow rate to see how increasing the flow rate affects the results. The comparison between the three conditions ($V_{mean} = 268$ µm/s, $1.5 \times V_{mean}$, and $2 \times V_{mean}$, the syringe pump is set to 0.014, 0.021, and 0.0315 µl/s) is shown in Fig. 11. As can be seen, the deviations in C1 results are significantly higher at faster flow rates ($\pm$ 2.33, 20.88 and 13.92 µm for 268, 402 and 536 µm/s
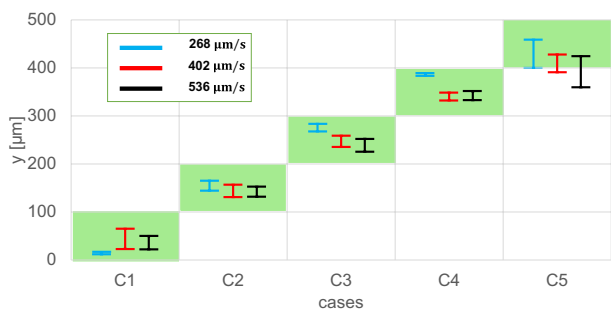

Fig. 11 The median value and the mean absolute deviation of the 5 cases for three conditions ($V_{mean} = 268 \mu$ m/s, $1.5 \times V_{mean}$, and $2 \times V_{mean}$)

respectively), due to insufficient operating time to pull down the incoming particles with higher y values, since in this case, the particles leave the ROI at the vertical side before reaching the horizontal side (y_t). In contrast to the minor increase in deviations in C2–C4, we find that the particles are positioned at lower levels compared to the results at 268 µm/s.

By increasing the Poiseuille flow/microstreaming ratio, the topology of the flow changes, and the lateral streaming is reduced, so the ROIs should be positioned slightly higher to compensate for this deficiency. This shows the importance of tuning the system for different flow rates at the beginning of the operation. Unlike previous cases where the deviations were still within the green target range (even with some changes in their amount), the particles of C5 could not be successfully positioned and the deviation exceeded the target range when the flow rate was increased. As expected, increasing the flow rate restricts the area far from the bubble where upward flow could enter at lower flow rates. Using multiple microbubbles on the opposite side of the microchannel could be an alternative approach to extend the range of lateral positioning (wider channel) and improve results at higher flow rates, where positioning occurs in multiple steps.

5 Conclusion

Here we presented an automated microfluidic bead sorter with an accuracy of up to tens of micrometers in single particle positioning, which does not require additional structures to precondition the flow for particle positioning (e.g., prefocusing of particles using sheath flows). Using the controlled microstreaming as a positioning operator, a variety of small particles can be precisely sorted across the width of the microchannel, which cannot be readily achieved in applications using an external on-off force. The positioning does not rely on particle-specific properties such as size, shape, density, compressibility, etc. so this approach is universally applicable in all areas of microfluidics. As the concept is not based on moving parts, just an oscillating bubble, the positioning device is robust and does not require any special maintenance or cleaning operations. Due to the optical analysis of the particle position this technology is limited to transparent fluids. Furthermore, the concept requires low numbers of particles to guarantee reliable positioning.

The following are some of our new findings in this work:

- We used non-invasive and non-destructive microbubble streaming in our positioning technique which is essential for biological cell application. The use of a high-power laser in optical tweezers, a large heat sink in plasmonic tweezers, and a high electric field in electrokinetic tweezers could seriously damage the cell

membrane or alter the natural experimental environment. Furthermore, these approaches are more complex compared to the microbubble streaming approach.

- Single particle positioning accuracies as high as high as $MAD_f = 2.3\,\mu m$ in a $500\,\mu m$ microchannel were achieved.
- A fast and highly tunable control system has been developed that operates effectively in live mode, allowing an operator to use it at the desired time to localize the particles, which is crucial when isolating rare cells or removing unwanted impurities in a flow.
- The technique is also applicable to non-fluorescent particles (no labeling required as long as the objects in the flow do not perfectly match the index of refraction of the flow medium).
- Compared to other methods, which are usually applicable for particles with a size of 1–$10\,\mu m$, the use of a relatively strong microstreaming makes this technique suitable for a wider range of particle sizes with higher Stokes numbers.

Declaration

Conflict of interest There are no conflicts to declare.

References

Ahmed D, Mao X, Juluri BK, Huang TJ (2009) A fast microfluidic mixer based on acoustically driven sidewall-trapped microbubbles. Microfluid Nanofluid 7(5):727

Ahmed D, Ozcelik A, Bojanala N, Nama N, Upadhyay A, Chen Y, Hanna-Rose W, Huang TJ (2016) Rotational manipulation of single cells and organisms using acoustic waves. Nat Commun 7(1):1–11

Armstrong AJ, Marengo MS, Oltean S, Kemeny G, Bitting RL, Turnbull JD, Herold CI, Marcom PK, George DJ, Garcia-Blanco MA (2011) Circulating tumor cells from patients with advanced prostate and breast cancer display both epithelial and mesenchymal markers. Mol Cancer Res 9(8):997–1007

Augustsson P, Karlsen JT, Su H-W, Bruus H, Voldman J (2016) Iso-acoustic focusing of cells for size-insensitive acousto-mechanical phenotyping. Nat Commun 7(1):1–9

Barnkob R, Kähler CJ, Rossi M (2015) General defocusing particle tracking. Lab Chip 15(17):3556–3560

Bischoff FZ, Marquez-Do D, Martinez D, Dang D, Horne C, Lewis D, Simpson J (2003) Intact fetal cell isolation from maternal blood: improved isolation using a simple whole blood progenitor cell enrichment approach (rosettesep^{TM}). Clin Genet 63(6):483–489

Chen J, Zheng Y, Tan Q, Zhang YL, Li J, Geddie WR, Jewett MA, Sun Y (2011) A microfluidic device for simultaneous electrical and mechanical measurements on single cells. Biomicrofluidics 5(1):014113

Chen Y, Li P, Huang P-H, Xie Y, Mai JD, Wang L, Nguyen N-T, Huang TJ (2014) Rare cell isolation and analysis in microfluidics. Lab Chip 14(4):626–645

Chen Y, Chung AJ, Wu T-H, Teitell MA, Di Carlo D, Chiou P-Y (2014) Pulsed laser activated cell sorting with three dimensional sheathless inertial focusing. Small 10(9):1746–1751

Cho S, Thielecke H (2007) Micro hole-based cell chip with impedance spectroscopy. Biosens Bioelectron 22(8):1764–1768

Collins DJ, Morahan B, Garcia-Bustos J, Doerig C, Plebanski M, Neild A (2015) Two-dimensional single-cell patterning with one cell per well driven by surface acoustic waves. Nat Commun 6(1):1–11

Collins DJ, Neild A, Ai Y (2016) Highly focused high-frequency travelling surface acoustic waves (saw) for rapid single-particle sorting. Lab Chip 16(3):471–479

Creber S, Pintelon T, Von Der Schulenburg DG, Vrouwenvelder J, Van Loosdrecht M, Johns M (2010) Magnetic resonance imaging and 3d simulation studies of biofilm accumulation and cleaning on reverse osmosis membranes. Food Bioprod Process 88(4):401–408

Flemming H-C (1997) Reverse osmosis membrane biofouling. Exp Thermal Fluid Sci 14(4):382–391

Han A, Frazier AB (2006) Ion channel characterization using single cell impedance spectroscopy. Lab Chip 6(11):1412–1414

Khine M, Lau A, Ionescu-Zanetti C, Seo J, Lee LP (2005) A single cell electroporation chip. Lab Chip 5(1):38–43

Klapper I, Dockery J (2010) Mathematical description of microbial biofilms. SIAM Rev 52(2):221–265

Malleo D, Nevill JT, Lee LP, Morgan H (2010) Continuous differential impedance spectroscopy of single cells. Microfluid Nanofluid 9(2–3):191–198

Marmottant P, Hilgenfeldt S (2003) Controlled vesicle deformation and lysis by single oscillating bubbles. Nature 423(6936):153–156

Mernier G, Piacentini N, Braschler T, Demierre N, Renaud P (2010) Continuous-flow electrical lysis device with integrated control by dielectrophoretic cell sorting. Lab Chip 10(16):2077–2082

Nan L, Jiang Z, Wei X (2014) Emerging microfluidic devices for cell lysis: a review. Lab Chip 14(6):1060–1073

Nilsson J, Evander M, Hammarström B, Laurell T (2009) Review of cell and particle trapping in microfluidic systems. Anal Chim Acta 649(2):141–157

Patel MV, Tovar AR, Lee AP (2012) Lateral cavity acoustic transducer as an on-chip cell/particle microfluidic switch. Lab Chip 12(1):139–145

Rahmati AR, Akbari OA, Marzban A, Toghraie D, Karimi R, Pourfattah F (2018) Simultaneous investigations the effects of non-newtonian nanofluid flow in different volume fractions of solid

nanoparticles with slip and no-slip boundary conditions. Therm Sci Eng Progress 5:263–277

Rallabandi B, Wang C, Hilgenfeldt S (2014) Two-dimensional streaming flows driven by sessile semicylindrical microbubbles. J Fluid Mech 739:57

Riley N (2001) Steady streaming. Annu Rev Fluid Mech 33(1):43–65

Sheng W, Ogunwobi OO, Chen T, Zhang J, George TJ, Liu C, Fan ZH (2014) Capture, release and culture of circulating tumor cells from pancreatic cancer patients using an enhanced mixing chip. Lab Chip 14(1):89–98

Shields CW IV, Reyes CD, López GP (2015) Microfluidic cell sorting: a review of the advances in the separation of cells from debulking to rare cell isolation. Lab Chip 15(5):1230–1249

Tchbanoglous G, Burton FL, Stensel HD (2003) Wastewater engineering: treatment and reuse. McGraw-Hill, Hoboken

Thameem R, Rallabandi B, Hilgenfeldt S (2016) Particle migration and sorting in microbubble streaming flows. Biomicrofluidics 10(1):014124

Toghraie Semiromi D, Azimian A (2010) Nanoscale poiseuille flow and effects of modified lennard-jones potential function. Heat Mass Transf 46(7):791–801

Tovar AR, Lee AP (2009) Lateral cavity acoustic transducer. Lab Chip 9(1):41–43

Versluis M, Goertz DE, Palanchon P, Heitman IL, van der Meer SM, Dollet B, de Jong N, Lohse D (2010) Microbubble shape oscillations excited through ultrasonic parametric driving. Phys Rev E 82(2):026321

Volk A, Kähler CJ (2018) Size control of sessile microbubbles for reproducibly driven acoustic streaming. Phys Rev Appl 9(5):054015

Volk A, Rossi M, Kähler CJ, Hilgenfeldt S, Marin A (2015) Growth control of sessile microbubbles in pdms devices. Lab Chip 15(24):4607–4613

Volk A, Rossi, M, Mutsch B, Kähler C (2019) Experimental investigation of oscillation modes and streaming of an acoustically actuated bubble in a microchannel. In: 32nd international congress on high-speed imaging and photonics, vol 11051, p 110510. International Society for Optics and Photonics

Vrouwenvelder J, Von Der Schulenburg DG, Kruithof J, Johns M, Van Loosdrecht M (2009) Biofouling of spiral-wound nanofiltration and reverse osmosis membranes: a feed spacer problem. Water Res 43(3):583–594

Wang C, Jalikop SV, Hilgenfeldt S (2012) Efficient manipulation of microparticles in bubble streaming flows. Biomicrofluidics 6(1):012801

Wang C, Rallabandi B, Hilgenfeldt S (2013) Frequency dependence and frequency control of microbubble streaming flows. Phys Fluids 25(2):022002

Wognum AW, Eaves AC, Thomas TE (2003) Identification and isolation of hematopoietic stem cells. Arch Med Res 34(6):461–475

Xia Y, Whitesides GM (1998) Soft lithography. Annu Rev Mater Sci 28(1):153–184

Yang S, Ündar A, Zahn JD (2006) A microfluidic device for continuous, real time blood plasma separation. Lab Chip 6(7):871–880

Zhao M, Schiro PG, Kuo JS, Koehler KM, Sabath DE, Popov V, Feng Q, Chiu DT (2013) An automated high-throughput counting method for screening circulating tumor cells in peripheral blood. Anal Chem 85(4):2465–2471